09,04

# Paramagnetic $Tb^{3+}$ centers in yttrium aluminum garnet

© G.R. Asatryan[1], G.S. Shakurov[2], N.G. Romanov[1], A.G. Petrosyan[3]

[1] Ioffe Institute,
St. Petersburg, Russia
[2] Zavoisky Physical-Technical Institute, FRC Kazan Scientific Center of RAS,
Kazan, Russia
[3] Institute for Physical Research, National Academy of Sciences of Armenia,
Ashtarak, Armenia

E-mail: hike.asatryan@mail.ioffe.ru

*Received January 11, 2024*
*Revised January 11, 2024*
*Accepted January 15, 2024*

Yttrium-aluminum garnet crystals with terbium impurity were studied by high-frequency EPR in a wide frequency range (70−200 GHz). Along with the $Tb^{3+}$ ions located in the yttrium position in a regular environment, a number of terbium centers with a lower concentration and changed values of the initial splitting of the non-Kramers quasi-doublets were observed. The change in the initial splitting is associated with the presence of antisite defects in the terbium environment. The terbium centers with a smaller initial splitting as compared to the main $Tb^{3+}$ were found and attributed to terbium ions, near which there are $Al_Y$ antisite defects (aluminum ions in dodecahedral positions of yttrium).

**Keywords:** electron paramagnetic resonance, yttrium aluminum garnet, rare earth elements, terbium, antisite defects.

DOI: 10.61011/PSS.2024.02.57925.2

## 1. Introduction

Studying the actual structure of yttrium aluminum garnet crystals $Y_3Al_5O_{12}$ (YAG) activated by rare earth ions is an important task. Such crystals are widely used in quantum electronics and optoelectronics, in nuclear physics and medical diagnostics, and are also considered promising for quantum computing systems [1–5].

$Tb^{3+}$ has a large set of fluorescence lines that provide a bright luminescence of phosphors used in cathode ray tubes and projection screens [6], in the yellow-green region. The research results of the luminescent properties of YAG:Tb phosphors in the form of single-crystals and ceramics are described in numerous papers (see, for example, [7–9]). With direct excitation of the upper level $^5D_4$ of $Tb^{3+}$ ions using blue highly efficient semiconductor InGaN light-emitting diodes (LED) with a wavelength of about 460 nm, a laser generation was obtained on the yellow and green lines of $Tb^{3+}$ in crystals of fluorides [10,11]. Yellow laser light is relevant in medicine for the treatment of skin and eye diseases. To date, laser generation of $Tb^{3+}$ ions was not obtained in oxide crystals, which indicates the need for further spectroscopic studies, as well as a detailed analysis of crystal lattice defects.

YAG:Ce is an industrial scintillator and phosphor that emits at the transition $5d-4f$ of $Ce^{3+}$ ions in a wide band with a maximum at 550 nm. In YAG:Ce,Tb [12] and LuAG:Ce,Tb [13] garnets the energy transfer $Tb^{3+} \rightarrow Ce^{3+}$ was registered, however, no increase in light output was observed. Among the reasons, the electron capture at crystal lattice defects was considered [13]. YAG:Ce is the most common phosphor for white LEDs, in which blue emission from InGaN is absorbed by cerium ions and converted into broad and intense emission in the yellow region. White light is achieved by mixing yellow light and unabsorbed portion of blue light. To improve the color rendering index of YAG:Ce the coactivators are used, including terbium ions, and due to the energy transfer of $Tb^{3+} \rightarrow Ce^{3+}$ the emission spectrum is supplemented with a red component (see, for example, paper [14], in which YAG:Ce,Tb single-crystal grown by the Czochralski method was studied).

Theoretical calculation of the formation energy of various defects in YAG crystals showed that antisite defects are predominant among intrinsic defects [15,16]. In YAG crystals they are formed during growth from a melt at high temperature as a result of replacement of $Al^{3+}$ ions by $Y^{3+}$ ($Y_{Al}$) ions, or $Y^{3+}$ ions at dodecahedral *c*-sites by $Al^{3+}$ ($Al_Y$) ions. Antisite defects are not paramagnetic and therefore can not be directly studied by electron paramagnetic resonance (EPR). However, they influence the environment of paramagnetic centers [17] and can change their spectra. Of particular interest for the study of antisite defects in garnet crystals is the study of EPR of $Tb^{3+}$ ions, for which the splitting of the levels of the non-Kramers quasi-doublet in zero field strongly depends on the symmetry of their environment, and, consequently, on the presence of defects near these ions.

The electronic configuration of $Tb^{3+}$ is $4f^8$, the ground state of free ion — $^7F_6$. In a crystal field, its ground state

**Table 1.** $g$-factors, values of level splitting in a zero magnetic field $\Delta$ and hyperfine interaction constants A of single ions $Tb^{3+}$ in various systems, determined by the EPR method

| Crystal | $g_{\parallel}$ | $\Delta$ | | A | | Ref |
|---|---|---|---|---|---|---|
| | | $cm^{-1}$ | GHz | $cm^{-1}$ | GHz | |
| $Y(C_2H_5SO_4)_3 \cdot 9H_2O$ | 17.72 | 0.387 | 11.60 | 0.209 | 6.266 | [18,19] |
| $CaWO_4$ | 17.777 | 0.271 | 8.131 | 0.2096 | 6.284 | [20] |
| $CaF_2$ | 17.77 | 0.171 | 5.134 | 0.209 | 6.26 | [20] |
| | 17.28 | 1.056 | 31.67 | 0.203 | 6.10 | |
| $SrF_2$ | 17.95 | 0.480 | 14.4 | 0.211 | 6.33 | [21] |
| | 17.85 | 0.687 | 20.6 | 0.210 | 6.29 | |
| $LiYF_4$ | 17.7 | 0.933 | 27.98 | 0.209 | 6.26 | [22] |
| $La_2O_2S$ | 17.8 | 0.18 | 5.40 | 0.216 | 6.47 | [23] |
| LaND | 17.2 | 0.270 | 8.08 | 0.201 | 6.03 | [24] |
| $YBa_2Cu_3O_6$ | 17.9 | 0.237 | 7.1 | – | – | [25] |
| $KPb_2Cl_5$ | 16.2 | 1.601 | 48 | 0.203 | 6.10 | [26] |
| $Mg_2SiO_4$ | 15.8 | 6.501 | 194.9 | 0.182 | 5.45 | [27] |
| | 15.9 | 7.869 | 235.9 | 0.183 | 5.50 | |
| $YAlO_3$ | 17.55 | 0.143 | 4.29 | 0.209 | 6.28 | [28] |
| **YAG** | **15.65** | **2.705** | **81.1** | **0.183** | **5.50** | This study |
| LuAG | 15.27 | 3.659 | 109.7 | 0.172 | 5.16 | [29] |

is split into six doublets with $M_J = \pm 6, \pm 5, \ldots, \pm 1$ and a singlet with $M_J = 0$. The doublet $M_J = \pm 6$ has the lowest energy. In the crystal field of axial symmetry, an admixture of excited states leads to a decrease in the value of $g_{\parallel}$ relative to $g_{\parallel} = 18$ for the pure state $M_J = \pm 6$, and causes splitting of the levels of the ground state doublet [18–20]. The crystal field of lower symmetry leads to complete splitting of the $4f^8$ multiplet levels into singlet states, and the magnitude of the splitting between the lowest energy levels can reach tens and even hundreds of Gegahertz. In the garnet lattice, the local symmetry of the dodecahedral position occupied by the impurity terbium ion, is rhombic ($D_2$), and the ground state of the $Tb^{3+}$ ions is a quasi-doublet with a small (about $3\,cm^{-1}$) level splitting in zero magnetic field.

EPR spectra of $Tb^{3+}$ can be described using the effective spin $S = 1/2$, the anisotropic $g$-factor ($g_{\perp} \sim 0$) and the value of level splitting in zero magnetic field $\Delta$ [18]. Terbium has one stable isotope $^{159}Tb$ with natural content of 100% and nuclear spin $I = 3/2$, therefore, in its EPR spectra each electronic transition is split into four hyperfine structure (HFS) lines. This makes it possible to unambiguously identify terbium centers.

EPR studies of $Tb^{3+}$ ions are not numerous, although the first papers appeared in 1950s. This is due to the fact that to record their spectra, it is necessary that the energy of the microwave photon at the operating frequency of EPR spectrometer exceeds the initial level splitting $\Delta$. The parameters of $Tb^{3+}$ centers determined by the EPR method in various crystals are summarized in Table 1.

For the convenience of comparing the results of different studies, the values of $\Delta$ and $A$ are given in both $cm^{-1}$ and GHz units. In the papers [26–29] to study $Tb^{3+}$ a broadband EPR spectrometer operating in the range $37-850$ GHz was used.

In YAG crystals EPR of $Tb^{3+}$-centers was studied at frequencies of 94 and 130 GHz [30]. In addition to the main centers — $Tb^{3+}$ ions, located in regular environment in the dodecahedral position with local symmetry $D_2$, three terbium centers were observed with the values $\Delta$ larger than for basic terbium. The existence of such centers was explained by the presence of antisite defects of $Y_{Al}$ (yttrium ions in the octahedral positions of aluminum) near the $Tb^{3+}$ ions, replacing $Y^{3+}$ [30,31]. In crystals of lutetium aluminum garnet (LuAG), along with EPR of $Tb^{3+}$ ions in the dodecahedral position, weak satellite signals were also observed, the origin of which is associated with the formation of antisite defects of $Lu_{Al}$ in the environment of $Tb^{3+}$ [29].

This paper relates to the studies of a family of paramagnetic terbium centers in YAG crystals using EPR in a wide frequency range (of 70 to 200 GHz), which made it possible to detect new terbium centers associated with the presence in the environment of $Tb^{3+}$ both antisite defects $Y_{Al}$ and antisite defects $Al_Y$.

## 2. Samples and experiment procedure

Single-crystals $Y_3Al_5O_{12}$ : Ce,Tb were grown at a temperature of about 1940°C by vertical directional crystallization, developed by Kh.S. Bagdasarov in the 1960s [32] (modified Bridgman method) at the IPR NAS RA (Ashtarak, Republic of Armenia). The crystals were grown in molybdenum containers in a neutral reducing atmosphere ($Ar/H_2$) using high-purity (99.99%) oxides and along the crystallographic axis ⟨100⟩, optimal for the given growth geometry [33]. Other details of crystallization conditions are given in [34]. The cerium content in the crystals was 0.12 at.% relative to yttrium, and the terbium concentration was estimated to be approximately 0.1 at.%. Samples for EPR studies were cut from the central homogeneous regions of crystals, free from facets, which, due to differences in growth mechanisms, differ in chemical composition and lattice constant [35,36]. The samples were oriented using X-ray diffraction methods.

EPR spectra were recorded in the frequency range 70−200 GHz at liquid helium temperature using the broadband high-frequency EPR spectrometer developed at the Zavoisky Physical-Technical Institute in Kazan [37].

## 3. Experimental results and discussion thereof

### 3.1. EPR of $Tb^{3+}$ ions in $Y^{3+}$ positions with regular environment

EPR spectra of $Tb^{3+}$ are described by the spin Hamiltonian

$$\hat{H} = \mu_B \mathbf{SgB} + (\Delta_x S_x + \Delta_y S_y) + A S_z I_z, \qquad (1)$$

where $\mu_B$ is the Bohr magneton, $S = 1/2$ is the effective electron spin, $I = 3/2$ is the spin of the terbium nucleus. The first term in (1) describes the Zeeman interaction, the second is the splitting of electronic levels in zero magnetic field, and the last term is the hyperfine interaction with the constant $A$. For $Tb^{3+}$ in YAG the axis $z$ coincides with one of ⟨100⟩ axes.

The energy levels of $Tb^{3+}$ in a magnetic field are determined by the expression

$$W = \pm 1/2 \sqrt{\Delta^2 + (g_z \mu_B B_z + A I_z)^2}, \qquad (2)$$

where $\Delta = (\Delta_x^2 + \Delta_y^2)^{1/2}$ is the level splitting in zero field.

Measurements in wide frequency range and calculations of the frequency-field dependences of the EPR spectra made it possible to verify the parameters of the spin

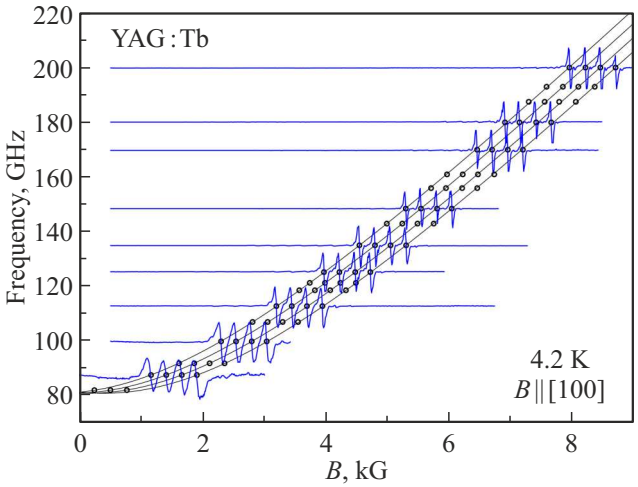


**Figure 1.** EPR spectra $Tb^{3+}$ in YAG, recorded at 4.2 K at different frequencies. The dots show the centers of the resonant lines in the spectra, the lines show the calculated frequency-field dependences of the resonant fields. $B \parallel [100]$.

Hamiltonian of $Tb^{3+}$ ions replacing $Y^{3+}$ at dodecahedral sites of the YAG lattice and having a regular environment: $g = 15.7$, $\Delta = 81.1$ GHz, $A = 5.5$ GHz. Figure 1 shows the frequency-field dependences of resonant transitions calculated using these parameters for the orientation $B \parallel [100]$. The dots mark the positions of the resonance lines of $Tb^{3+}$-centers. EPR spectra recorded at different frequencies are also shown. A good agreement between the calculated and experimental dependences is observed.

### 3.2. $Tb^{3+}$-centers in dodecahedral sites of the YAG lattice with antisite defects in their environment

Figure 2 shows EPR spectra of YAG : Tb crystals recorded at 4.2 K at frequencies of 95.7, 112.9, 125.3 and 170 GHz. Along with the EPR of the main centers of $Tb^{3+}$ replacing $Y^{3+}$ in the regular environment, signals with approximately 50 times lower intensity are observed. They are clearly visible in the spectra shown in enlarged scale. These spectra contain a large number of lines, the assignment of which to terbium centers is unambiguously determined by the observation of the hyperfine structure characteristic of terbium. Registration of EPR at many frequencies made it possible to identify centers with different initial splittings and determine their parameters using calculations of frequency-field dependencies, which are shown in Figure 3. The dots in this Figure correspond to the line positions in the EPR spectra. Open circles indicate the EPR lines of the main terbium centers.

The vertical lines in Figure 2 show the calculated positions of the EPR lines. The different terbium centers are marked by the value of the initial level splitting $\Delta$. In addition to the lines of the main terbium centers ($\Delta = 81.1$ GHz) and centers with $\Delta = 94.0$, 98.2

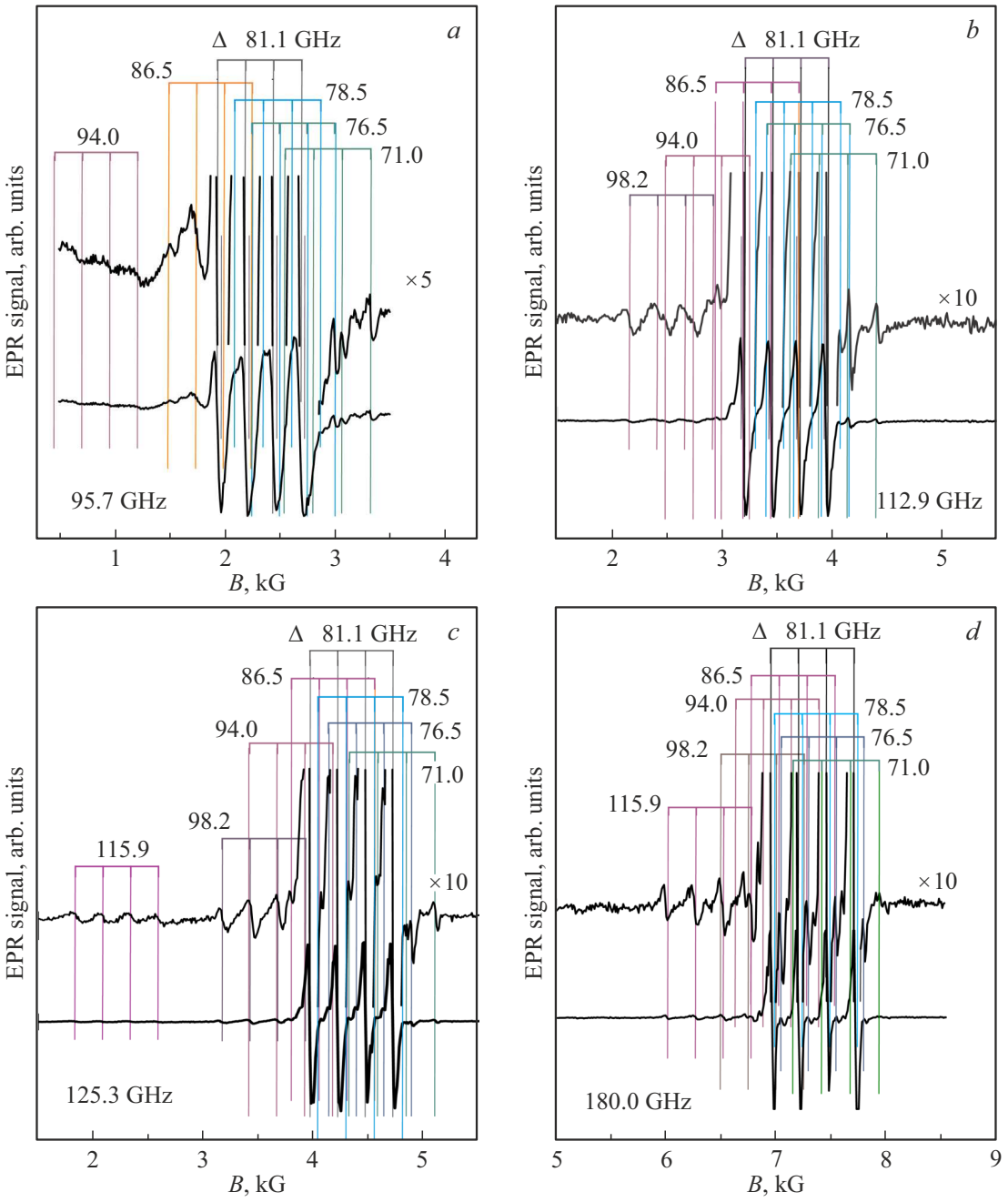


**Figure 2.** EPR spectra of $Tb^{3+}$-centers in YAG, recorded at frequencies *a*) 85.5 GHz, *b*) 112.9 GHz, *c*) 125.3 GHz and *d*) 180 GHz at 4.2 K in $B \parallel [100]$ orientation. The spectra of different types of terbium centers are indicated by the value of the initial level splitting Δ. Vertical lines mark the calculated positions of the lines of these centers.

and 115.9 GHz, corresponding to the centers $Tb^{3+}$(I), $Tb^{3+}$(II), $Tb^{3+}$(III) from Refs. [30,31], the EPR spectra contain lines of a number of new centers. Among them we can distinguish centers with $\Delta = 86.5$ GHz, as well as centers with less splitting: 71.0 GHz and 76.5 GHz and 78.5 GHz.

The parameters of terbium centers used in the calculations are summarized in Table 2.

The main centers — terbium ions, replacing $Y^{3+}$ in dodecahedral lattice sites and having a regular environment, are designated as $Tb^{3+}$. „Additional“ terbium centers are divided into groups A (centers with smaller initial splitting Δ) and B (centers with larger splitting Δ), respectively.

The orientation dependences of the resonant magnetic fields for the EPR signals of „additional“ terbium centers from groups A and B are similar to such dependences for the main $Tb^{3+}$ center, therefore these centers can be identified as $Tb^{3+}$ ions, located in the dodecahedral sites of the garnet lattice, which environment contains an antisite defect. Different values of the parameter Δ for these centers suggest different perturbations of the crystal field. Three

**Table 2.** $g$-factors, values of level splitting of a non-Kramers quasi-doublet in zero field $\Delta$ and hyperfine interaction constants $A$ $Tb^{3+}$-centers in YAG

| Center | $g$ | $\Delta$, GHz | $A$, GHz |
|---|---|---|---|
| $Tb^{3+}$ ($A1$) | 15.65 | 71.0 | 5.7 |
| $Tb^{3+}$ ($A2$) | 15.70 | 76.5 | 5.6 |
| $Tb^{3+}$ ($A3$) | 15.70 | 78.5 | 5.5 |
| **$Tb^{3+}$** | **15.65** | **81.1** | **5.5** |
| $Tb^{3+}$ ($B4$) | 15.65 | 86.5 | 5.5 |
| $Tb^{3+}$ ($B3$) | 15.60 | 94.0 | 5.5 |
| $Tb^{3+}$ ($B2$) | 15.60 | 98.2 | 5.5 |
| $Tb^{3+}$ ($B1$) | 15.36 | 115.9 | 5.4 |

types of centers ($B1, B2, B3$) with the largest values of $\Delta$ correspond to three values of the distances between the ion $Tb^{3+}$ and the nearest antisite defect $Y_{Al}$ „a“ of YAG [31]. Centers with a smaller deviation of $\Delta$ from 81.1 GHz correspond to more distant positions of antisite defects. These include the center with $\Delta = 86.5$ GHz, shown in Figure 2.

Previously, in EPR of YAG:Ce crystals measured at the orientation $B \parallel [100]$ we observed three „additional“ centers of $Ce^{3+}$ with $g$-factors smaller than $g$-factors of the main center, and two centers — with larger $g$-factors [17]. These centers were attributed to cerium ions having an antisite defect in their environment. The orientation dependences of EPR spectra of „additional“ centers of terbium and cerium show that the symmetry of their immediate environment does not undergo significant distortion [17,30]. From this we can assume that changes in the parameters of centers with a defect in the environment ($g$-factors for $Ce^{3+}$ and initial splittings in the case of $Tb^{3+}$) occur mainly due to changes in distances between the paramagnetic center and oxygen. When substituting $Y^{3+} \rightarrow Al^{3+}$ or $Al^{3+} \rightarrow Y^{3+}$ in the immediate environment of the impurity rare-earth ion, the distortions of its environment will fundamentally differ in the stretching or compression of oxygen polyhedra, respectively. In Ref. [31] it was concluded that the presence of an antisite defect of $Y_{Al}$-type near $Tb^{3+}$ leads to compression of the oxygen dodecahedron and the formation of predominantly three types of centers with initial splitting values greater than for the main center.

New EPR spectra found in this work in higher fields relative to the main $Tb^{3+}$ belong to centers for which the initial splitting $\Delta$ is less than that of terbium ions in regular positions. These spectra can be attributed to $Tb^{3+}$ ions, surrounded by antisite defects $Al_Y$ (aluminum in the yttrium position).

To estimate the number of types of such centers, the environment of the paramagnetic center in the YAG lattice was analyzed, and the positions of antisite defects of the type $Al_Y$ closest to $Tb^{3+}$ ($Y^{3+}$ ion substitution by aluminum $Al^{3+}$ with a significantly smaller ionic radius) were analyzed. Positions of nearest to $Tb^{3+}$ $Y_{Al}$-type antisite defects were considered in Ref. [31]. Figure 4 shows a fragment of a YAG lattice cell, which shows the dodecahedral positions of yttrium in the environment of the paramagnetic center. $Y^{3+}$ ions in these positions can be substituted by aluminum, forming antisite defects of $Al_Y$-type. For simplicity, aluminum ions (sites $a$ and $c$), as well as oxygen ions are not shown.

The distances from the paramagnetic center $Tb^{3+}$ to sites A and B are the same and equal to 3.66 Å. The distances to sites C and D are also the same (5.65 Å). The distance to the E and F sites located on the crystallographic axes [001] is 6.01 Å, and the distance to G and H sites is 6.73 Å. Considering that the sites E, F, G, H are located at a longer distance from $Tb^{3+}$ and do not have common

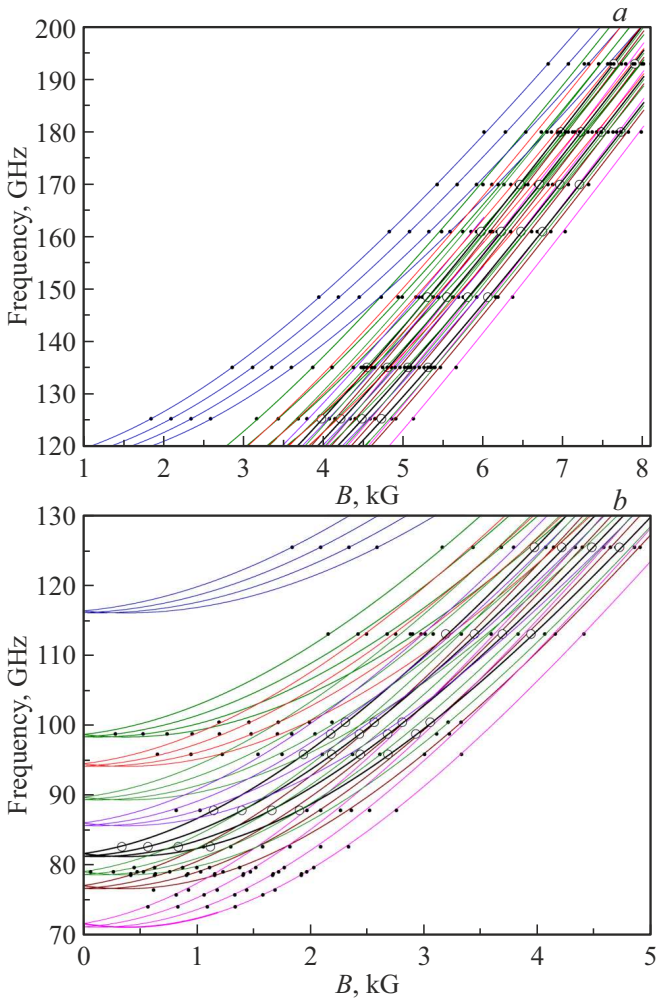


**Figure 3.** Calculated frequency-field dependences for terbium centers in YAG. The dots mark the position of the lines in the measured EPR spectra. The calculation results for the main centers $Tb^{3+}$ are shown by thick lines, and the experimental positions of the resonance lines for them are shown by open circles. Calculations were performed using (2) and the parameters of terbium centers given in Table 2.

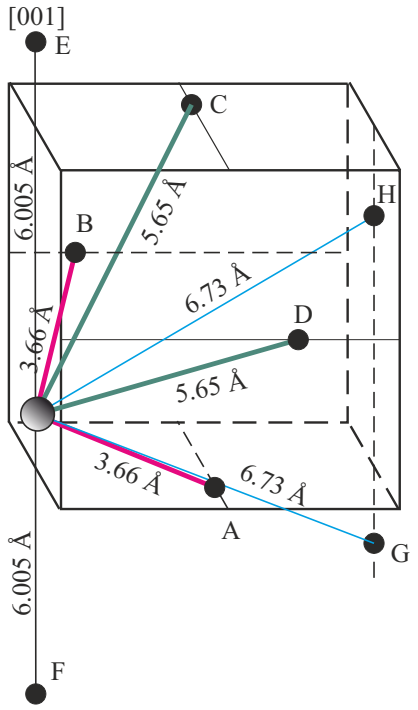


**Figure 4.** Fragment of YAG lattice cell. The yttrium dodecahedral sites in the environment of the paramagnetic center $Tb^{3+}$ — possible positions of antisite defects of the type $Al_Y$ are indicated, as well as their distances from $Tb^{3+}$. For simplicity, aluminum ions and oxygen ions are not shown.

oxygen ions with the paramagnetic center, their influence on the crystal field at the location of $Tb^{3+}$ and, therefore, on the value of $\Delta$ and the EPR spectra will be less significant. Thus, due to substitutions of sites A and B, C and D, two types of paramagnetic centers should predominate, for which the initial splitting is less than $\Delta$ of the main center, and have maximum difference from it. The values of $\Delta$ for terbium centers with antisite defects located at longer distance are closer to $\Delta$ of the main centers.

For $Tb^{3+}(B_3)$ centers with $\Delta = 94$ GHz EPR spectra were recorded in zero magnetic field and in weak magnetic fields using magnetic field modulation and electron spin echo [30]. In this paper, EPR signals near zero field were observed for several terbium centers. Their analysis requires additional studies.

## 4. Conclusion

Non-Kramers ions $Tb^{3+}$ in yttrium-aluminum garnet crystals were studied by high-frequency EPR in a wide frequency range (70–200 GHz). Along with the main signals of $Tb^{3+}$ ions located in the yttrium position with regular environment, a number of new centers with lower concentration and the values of the initial splitting of the levels of the non-Kramers quasi-doublet, both larger and smaller, than for regular terbium centers were observed. It was shown that in YAG:Tb there were at least three types of paramagnetic centers of $Tb^{3+}$:

1. $Tb^{3+}$ ions located in dodecahedral *c*-sites of the YAG lattice (in positions of $Y^{3+}$) in a regular environment.

2. $Tb^{3+}$ ions in positions of $Y^{3+}$, which environment contains an a $Y_{Al}$ antisite defect (yttrium substitutes aluminum in the octahedral sites of the YAG lattice).

3. Terbium ions, near which there is an antisite defect $Al_Y$ (aluminum ion in the dodecahedral positions of yttrium).

### Funding

The study was financially supported by the Russian Foundation for Basic Research (the RFBR grant No. 20-52-05002 Arm_a) and the Committee of Science of RA within the framework of the project No. 1-6 /23-I/IPR. The study at KPhTI FRC KazSC RAS was carried out within the framework of the Government assignment.

### Conflict of interest

The authors declare that they have no conflict of interest.

## References

[1] A.A. Kaminskii. Laser Crystals: Their Physics and Properties. Springer, Berlin (1990).
[2] V. Bachmann, C. Ronda, A. Meijerink. Chem. Mater. **21**,
[3] Y.S. Lin, R.S. Liu, B.-M. Cheng. J. Electrochem. Soc. **152**, *6*, J41 (2005).
[4] A.C. Dujardin, E. Auffray, E. Bourret-Courchesne, P. Dorenbos, P. Lecoq, M. Nikl, A.N. Vasil'ev, A. Yoshikawa, R.-Y. Zhu. IEEE Trans. Nucl. Sci. **65**, *8*, 1977 (2018).
[5] P. Slyushev, K. Xia, R. Reuter, M. Jamali, N. Zhao, N. Yang, C. Duan, N. Kukharchyk, A.D. Wieck, R. Kolesov, J. Wrachtrup. Nature Commun. **5**, *1*, 3895 (2014).
[6] I. Kandarakis, D. Cavouras, G.S. Panayiotakis, C.D. Nomicos. Phys. Med. Biol. **42**, *7*, 1351 (1997).
[7] D.J. Robbins, B. Cockayne, B. Lent, C.N. Duckworth, J.L. Glasper. Phys. Rev. B **19**, *2*, 1254 (1979).
[8] Y.C. Kang, I.W. Lenggoro, S.B. Park, K. Okuyama. J. Phys. Chem. Solids **60**, *11*, 1855 (1999).
[9] J. Dai, M. Cao, H. Kou, Y. Pan, J. Guo, J. Li. Ceram. Int. **42**, *12*, 13812 (2016).
[10] C. Kränkel, D.T. Marzahl, F. Moglia, G. Huber, P. Metz. Las. Photon. Rev. **10**, *4*, 548 (2016).
[11] S. Kalusniak, E. Castellano-Hernandez, H. Yalçinoğlu, H. Tanaka, C. Kränkel. Appl. Phys. B **128**, *2*, 33 (2022).
[12] V. Khanin, A.-M. van Dongen, D. Buettner, C. Ronda, P. Rodnyi. ECS J. Solid State Sci. Technol. **4**, *8*, R128 (2015).
[13] J.M. Ogiegło, A. Zych, K.V. Ivanovskikh, T. Jüstel, C.R. Ronda, A. Meijerink. J. Phys. Chem. A **116**, *33*, 8464 (2012).
[14] M. Gong, W. Xiang, X. Liang, J. Zhong, D. Chen, J. Huang, G. Gu, C. Yang, R. Xiang. J. Alloys. Compounds **639**, 611 (2015).
[15] M.M. Kuklja. J. Phys.: Condens. Matter **12**, *13*, 2953 (2000).
[16] B. Liu, M. Gu, X. Liu, S. Huang, C. Ni. Appl. Phys. Lett. **94**, *12*, 121910 (2009).

[17] G.R. Asatryan, D.D. Kramushchenko, Yu.A. Uspenskaya, P.G. Baranov, A.G. Petrosyan. Phys. Solid State **56**, *6*, 1150 (2014).
[18] A. Abraham, B. Bleaney. Electron Paramagnetic Resonance of Transition Ions. Clarendon, Oxford (1970).
[19] J.M. Baker, B. Bleaney. Proc. Phys. Soc. A **68**, *3*, 257 (1955).
[20] P.A. Forrester, C.F. Hempstead. Phys. Rev. **126**, *3*, 923 (1962).
[21] A.A. Antipin, L.D. Livanova, L.Ya. Shekun. FTT **10**, *5*, 1286 (1968). (in Russian).
[22] I. Laursen, L.M. Holmes. J. Phys. C **7**, *20*, 3765 (1974).
[23] J.W. Jewett, P.E. Wigen. J. Chem. Phys. **61**, *8*, 2991 (1974).
[24] J.M. Baker, C.A. Hutchison, M.J.M. Leask, P.M. Martineau, M.G. Robinson, M.R. Wells. Proceed. R. Soc. Lond. A **413**, *1845*, 515 (1987).
[25] M.R. Gafurov, V.A. Ivanshin, I.N. Kurkin, M.P. Rodionova, H. Keller, M. Gutmann, U. Staub. J. Superconductivity. Nov. Magn. **13**, *6*, 895 (2000).
[26] G.S. Shakurov, B.Z. Malkin, A.R. Zakirov, A.G. Okhrimchuk, L.N. Butvina, N.V. Lichkova, V.N. Zavgorodnev. Appl. Magn. Res. **26**, *4*, 579 (2004).
[27] A.A. Konovalov, D.A. Lis, K.A. Subbotin, V.F. Tarasov, E.V. Zharikov. Appl. Magn. Reson. **45**, *2*, 193 (2014).
[28] G.R. Asatryan, G.S. Shakurov, I.V. Il'in, A.G. Petrosyan, K.L. Ovanesyan, M.V. Derdzyan. Phys. Solid State **63**, *12*, 1879 (2021).
[29] G.R. Asatryan, G.S. Shakurov, K.L. Hovhannesyan, A.G. Petrosyan. Phys. Solid State **65**, *3*, 406 (2023).
[30] E.V. Edinach, Y.A. Uspenskaya, A.S. Gurin, R.A. Babunts, H.R. Asatryan, N.G. Romanov, A.G. Badalyan, P.G. Baranov. Phys. Rev. B **100**, *10*, 104435 (2019).
[31] G.R. Asatryan, E.V. Edinach, Yu.A. Uspenskaya, R.A. Babunts, A.G. Badalyan, N.G. Romanov, A.G. Petrosyan, P.G. Baranov. Phys. Solid State **62**, *11*, 2110 (2020).
[32] Kh.S. Bagdasarov. Kristallizatsiya iz rasplava. Sovremennaya kristallografiya / Pod red. B.K. Vaynshtein. Nauka, M. (1980). T. 3. S. 337. (In Russian).
[33] A.G. Petrosyan. J. Cryst.Growth **139**, *3–4*, 372 (1994).
[34] A.G. Petrosyan, G.O. Shirinyan, K.L. Ovanesyan, A.A. Avetisyan. Cryst. Res. Technol. **13**, *1*, 43 (1978).
[35] B. Cockayne, J.M. Roslington, A.W. Vere. J. Mater. Sci. **8**, *3*, 382 (1973).
[36] A.A. Chernov. Ann. Rev. Mater. Res. **3**, 397 (1973).
[37] V.F. Tarasov, G.S. Shakurov. Appl. Magn. Reson. **2**, *3*, 571 (1991).

*Translated by I.Mazurov*